Theoretical, Spectroscopic, and Electrochemical Studies of Tetracobalt, Tetrarhodium, and Tetrairidium Dodecacarbonyl and Tris(diphenylphosphino)methane-Substituted Derivatives

Gary F. Holland,[1a] Donald E. Ellis,*[1a] David R. Tyler,[1b] Harry B. Gray,*[1b] and William C. Trogler*[1c]

Contribution from the Chemistry Department, Northwestern University, Evanston, Illinois 60201, Arthur Amos Noyes Laboratory, California Institute of Technology, Pasadena, California 91125, and Department of Chemistry, D-006, University of California at San Diego, La Jolla, California 92093. *Received October 27, 1986*

Abstract: Optical spectra and cyclic voltammograms of $M_4(CO)_{12}$ and $M_4(CO)_9[(PPh_2)_3CH]$ clusters have been measured, where M = Co, Rh, and Ir. For the $M_4(CO)_{12}$ complexes SCF-Xα-DV calculations were performed to examine bonding trends and to aid in assignment of their spectra. All cluster complexes exhibit a metal-localized $\sigma \rightarrow \sigma^*$ transition, at 375 nm in $Co_4(CO)_{12}$, 303 nm in $Rh_4(CO)_{12}$, and 321 nm in $Ir_4(CO)_{12}$. All clusters are calculated to contain similar LUMO's with $7a_2$ and 27e in the C_{3v} clusters (M = Co, Rh) correlating with the $9t_1$ LUMO in T_d symmetry $Ir_4(CO)_{12}$. The energy ordering for this transition, Co < Ir < Rh, is reversed from what might be expected because of increased metal-metal bonding on descending a metal triad; however, the order agrees with calculated band positions (Co, 393 nm; Ir, 350 nm; Rh, 274 nm). The inverted order for Rh and Ir is attributed to the structural change $C_{3v} \rightarrow T_d$ on progressing from $Rh_4(CO)_{12}$ to $Ir_4(CO)_{12}$ where three bridging carbonyls become terminal. Coordination of the $(PPh_2)_3CH$ ligand decreases the energy of the $\sigma \rightarrow \sigma^*$ transition by 350-6000 cm^{-1} in these clusters. The Xα calculations also accurately model the splitting between metal d band and carbonyl peaks in the UPS spectra of $M_4(CO)_{12}$ clusters. Calculated splittings within the d band are 2.5-3 eV for M = Co, 3.0-3.5 eV for M = Rh, and 6 eV for M = Ir. This reflects the increasing metal-metal interactions on descending the triad. Calculated charges for the M_4 core in the $M_4(CO)_{12}$ clusters show the Rh_4 (+5.39) and Ir_4 (+5.40) cores to be much more electron deficient than Co_4 (+3.11). In a previous study it was found that cluster core charges correlated well with redox potentials as ligands are changed around a common metal core. A similar correlation does not hold for a change in metal core and is attributed to changing covalent metal-metal interactions that are not reflected in the values of core charges.

Tetranuclear carbonyl clusters of formula $M_4(CO)_{12}$ (M = Co, Rh, Ir) exhibit rich substitution, catalytic, and structural chemistry.[2] As the simplest carbonyl clusters to show three-dimensional metal-metal bonding, it is important to understand their electronic structure. The isostructural cobalt and rhodium clusters,[3] of C_{3v} symmetry, contain three carbonyls bridging three equivalent metals in the basal plane (Figure 1a). The analogous iridium cluster adopts T_d symmetry containing three terminal carbonyls per Ir (Figure 1b).[4] Substitution of CO groups with phosphine donor ligands often leads to an intramolecular rearrangement for $Ir_4(CO)_{12}$ with some terminal carbonyl groups moving to bridging sites.[5]

Experimental limitations hamper comparisons of the electronic structures of the $M_4(CO)_{12}$ clusters. Poor solubility in most solvents and poor stability toward CO substitution[6] limit solution studies of $Ir_4(CO)_{12}$. Instability of $Rh_4(CO)_{12}$ toward decomposition to octahedral $Rh_6(CO)_{16}$ or other higher nuclearity rhodium clusters[7] hinders study of its physical properties. Synthesis of the tridentate ligand $(PPh_2)_3CH$[8,9] (tripod) and preparation of its adducts with cluster carbonyls[10] provide a convenient method for making stable and soluble derivatives of the $M_4(CO)_{12}$ clusters. Coordination of the tripod ligand to form $M_4(CO)_9$(tripod) enhances stability of the M = Rh and Co clusters, and it yields a soluble M = Ir cluster. Furthermore, crystallographic studies have revealed that coordination of tripod involves simple CO substitution, without extensive cluster rearrangement.[10] Thus the cobalt and rhodium clusters retain three bridging carbonyls in the basal (tripod capped) plane, while the Ir cluster remains free of carbonyl-bridged metal-metal bonds.[10]

In previous work we described[11] the similarities between $Co_4(CO)_{12}$ and the substituted $Co_4(CO)_9[(PPh_2)_3CH]$ derivative. With an understanding of the tripod ligand effects for a single metal cluster core, we now use calculations of the $M_4(CO)_{12}$ species in concert with experimental measurements for $M_4(CO)_{12}$ and $M_4(CO)_9$(tripod) compounds to define periodic trends for tetrahedral carbonyl clusters. The enhanced cluster stability afforded by tripod substitution permits a combination of electrochemical, spectroscopic, and theoretical techniques to be employed. Calculations using the SCF-Xα-DV[12] method, instrumental in our understanding[11,13] of $Ru_3(CO)_{12}$, $Os_3(CO)_{12}$, and tetracobalt carbonyl clusters, have been performed to provide a framework for the interpretation of spectroscopic and electrochemical properties, as well as provide a quantitative analysis of bonding in these clusters. Besides yielding information relevant to an understanding of the photochemistry of carbonyl clusters,[14] such calculations have also been used[15] to explain the magnetism of small clusters as molecular models for small metallic particles. A density of states (DOS) analysis of bonding that has proved so useful in a molecular understanding of the bonding in extended

(1) (a) Northwestern University. (b) California Institute of Technology. (c) University of California at San Diego.
(2) Adams, R. D.; Horvath, I. T. *Prog. Inorg. Chem.* **1985**, *33*, 127-181.
(3) Wei, C. H. *Inorg. Chem.* **1969**, *8*, 2384-2397.
(4) Churchill, M. R.; Hutchinson, J. P. *Inorg. Chem.* **1978**, *17*, 3528-3535.
(5) Muetterties, E. L.; Burch, R. R.; Stolzenberg, A. M. *Annu. Rev. Phys. Chem.* **1982**, *33*, 89-118.
(6) Stuntz, G. F.; Shapley, J. R. *Inorg. Chem.* **1976**, *15*, 1994-1996 and references therein.
(7) Garlaschelli, L.; Chini, P.; Martinengo, S. *Gazz. Chim. Ital.* **1982**, *112*, 285-288.
(8) Abbreviations: $(PPh_2)_3CH$, tripod; Ph, C_6H_5.
(9) Issleib, V. K.; Abicht, H. P. *J. Prakt. Chem.* **1970**, *312*, 456-465.
(10) Arduini, A. A.; Bahsoun, A. A.; Osborne, J. A.; Voelker, C. *Angew. Chem., Int. Ed. Engl.* **1980**, *19*, 1024-1025. Bahsoun, A. A.; Osborne, J. A.; Voelker, C.; Bonnet, J. J.; Lavigne, G. *Organometallics* **1982**, *1*, 1114-1120. Bahsoun, A. A.; Osborne, J. A.; Kintzinger, J.-P.; Bird, P. H.; Siriwardane, U. *Nouv. J. Chim.* **1984**, *8*, 125-132. Harding, M. M.; Nicholls, B. S.; Smith, A. K. *J. Organomet. Chem.* **1982**, *226*, C17-C20. Clucas, J. H.; Harding, M. M.; Nicholls, B. S.; Smith, A. K. *J. Chem. Soc., Chem. Commun.* **1984**, 319-320. Darensbourg, D. J.; Zalewski, D. J.; Rheingold, A. L.; Durney, R. L. *Inorg. Chem.* **1986**, *25*, 3281-3290.
(11) Holland, G. F.; Ellis, D. E.; Trogler, W. C. *J. Am. Chem. Soc.* **1986**, *108*, 1884-1894.
(12) (a) Ellis, D. E.; Painter, G. S. *Phys. Rev. B: Solid State* **1970**, *2*, 2887-2889. (b) Delley, B.; Ellis, D. E. *J. Chem. Phys.* **1982**, *76*, 1949-1960.
(13) Delley, B.; Manning, M. C.; Berkowitz, J.; Ellis, D. E.; Trogler, W. C. *Inorg. Chem.* **1982**, *21*, 2247-2253.
(14) Bentsen, J. G.; Wrighton, M. S., submitted for publication. Tyler, D. R.; Altobelli M.; Gray, H. B. *J. Am. Chem. Soc.* **1980**, *102*, 3022-3024.
(15) Johnson, D. C.; Benfield, R. E.; Edwards, P. O.; Nelson, W. J. H.; Vargas, M. D. *Nature* (London) **1985**, *314*, 231-235.

0002-7863/87/1509-4276$01.50/0

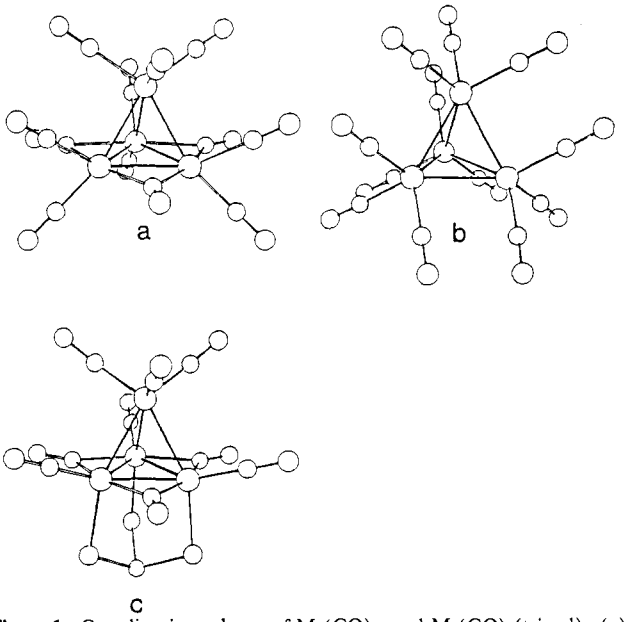

Figure 1. Coordination spheres of $M_4(CO)_{12}$ and $M_4(CO)_9$(tripod): (a) $Co_4(CO)_{12}$ and $Rh_4(CO)_{12}$; (b) $Ir_4(CO)_{12}$; (c) $Co_4(CO)_9$(tripod) and $Rh_4(CO)_9$(tripod); the analogous Ir complex has all terminal CO groups.

solids[16] has been adopted for the analysis of bonding in these many electron clusters.

Experimental Section

Solvents were obtained from commercial sources, purified by standard methods,[17] distilled, and stored under N_2. All manipulations were performed under an inert atmosphere of prepurified N_2 by using modified Schlenk and vacuum line techniques. Tetrairidium dodecacarbonyl and tris(diphenylphosphino)methane were obtained from Strem Chemical Co. The clusters $Rh_4(CO)_{12}$,[18] $Rh_4(CO)_9$(tripod), and $Ir_4(CO)_9$(tripod)[10] were prepared according to published procedures, and [PPN][$Rh(CO)_4$] was generously donated by Mr. J. Hriljac. Infrared spectra were recorded with use of a Perkin-Elmer Model PE-283 spectrometer. Optical spectra were recorded (in a quartz cuvette fitted with a Teflon valve and Pyrex bulb) with use of a Perkin-Elmer PE-320 or PE-330 spectrophotometer; all solvents were triply freeze–pump–thaw degassed and vacuum distilled onto samples. The MCD spectra were measured on a Cary 61 spectropolarimeter. Magnetic circular dichroism measurements at fields of about 38 kG were obtained with use of a Varian superconducting magnet.

Electrochemistry. Electrochemical measurements were made with use of a Princeton Applied Research Corp. Model 173 potentiostat/galvanostat, Model 179 digital coulometer, Model 175 universal programmer, and Model RE0074 X-Y recorder. The potentiostat employed positive feedback circuitry to compensate for solution resistance. A one-compartment cell modified from a published design[19] was used in cyclic voltammetry experiments. It contained Pt disk working and Pt wire auxiliary electrodes as well as a Ag wire (AgRE) quasi-reference. The AgRE was found to have a reproducible potential of +0.31 V vs. SCE; all potentials are reported vs. AgRE. Bulk electrolyses, performed in a four-electrode, three-compartment cell modified from the design of Smith and Bard,[20] contained a Pt mesh electrolysis electrode, a Pt disk working electrode for CV, a coiled Pt wire auxiliary electrode, and Ag wire reference electrode. In a typical experiment, supporting electrolyte tetra-*n*-butylammonium tetrafluoroborate ($TBABF_4$, Aldrich) was weighed in air and transferred to the three compartments of the electrolysis cell and evacuated overnight at 10^{-6} torr. On a Schlenk line, sample was added to the working compartment against an N_2 flush. The cell was returned to the vacuum line and evacuated, and CH_2Cl_2 solvent was distilled into the cooled cell. Platinum electrodes were soaked in chromic acid solution when not in use and rinsed with distilled H_2O before an experiment. The Pt disk CV working electrode was polished with 0.3-μm alumina before each experiment. The AgRE was rinsed with concentrated nitric acid and then with distilled water before each experiment.

Table I. Mulliken Populations, Total Mulliken Charge ($M\rho$), and Volume Integrated Charge ($\int\rho$) for $M_4(CO)_{12}$ Clusters[a]

		M		
		Co[c]	Rh	Ir
M^{apical}	n[b]d	7.70	7.57	7.46
	$(n+1)$s	0.27	0.23	0.35
	$(n+1)$p	0.73	0.51	1.00
	$(n+1)$d	−0.16	−0.13	−0.06
	$M\rho$	+0.56	+0.08	+0.25
	$\int\rho$	+0.62	+1.17	+1.35
M^{basal}	nd	7.69	7.54	
	$(n+1)$s	0.25	0.18	
	$(n+1)$p	0.39	0.43	
	$(n+1)$d	−0.30	−0.27	
	$M\rho$	+1.00	+1.12	
	$\int\rho$	+0.83	+1.41	
C^{apical}	2s	1.30	1.40	1.13
	2p	2.42	2.51	2.76
	$M\rho$	+0.28	+0.09	+0.11
	$\int\rho$	+0.14	−0.01	−0.15
$C^{basal,term}$	2s	1.27	1.42	
	2p	2.63	2.55	
	$M\rho$	+0.10	+0.03	
	$\int\rho$	+0.05	−0.03	
O^{term}	2s	1.80	1.83	1.76
	2p	4.56	4.52	4.52
	$M\rho$	−0.36	−0.35	−0.28
	$\int\rho$	−0.32	−0.36	−0.30
C^{br}	2s	1.34	1.43	
	2p	2.72	2.72	
	$M\rho$	−0.06	−0.15	
	$\int\rho$	+0.02	−0.19	
O^{br}	2s	1.78	1.82	
	2p	4.55	4.51	
	$M\rho$	−0.33	−0.33	
	$\int\rho$	−0.36	−0.45	

[a] M^{apical} = unique apical M atom in C_{3v} symmetry; M^{basal} = atoms making up plane of three equivalent M's; C^{apical} = carbon of CO bonded to M^{apical}; $C^{basal,term}$ = carbon of terminal CO group bonded to M^{basal}; O^{term} = oxygen bonded to C^{apical} or $C^{basal,term}$; C^{br}, O^{br} = atoms in bridging carbonyl sites. [b] n = 3, 4, and 5 for Co, Rh, and Ir, respectively. [c] Data from ref 13.

Calculations. Nonrelativistic, one-electron, self-consistent field (SCF) molecular energy levels were calculated for $Co_4(CO)_{12}$,[11] $Rh_4(CO)_{12}$, and $Ir_4(CO)_{12}$ by using the Xα–DV method.[12] An exchange parameter of 0.70 was used in all calculations. Numerical orbitals[21] were used throughout as basis functions. For Rh, all orbitals $1s^2...4d^8\,5s^1\,5p^0\,5d^0$ were included; a $1s^2...4f^{14}\,5d^8\,6s^1\,6p^0\,6d^0$ basis was used for Ir, and a potential well was used for the metals to localize virtual orbitals. A minimal 1s, 2s, 2p basis was used for carbon and oxygen. Valence orbitals were orthogonalized explicitly against frozen core orbitals (1s through 4p on Rh, 1s through 4f on Ir, 1s on C and O). Atomic populations were calculated by use of the Mulliken scheme.[22] Preliminary calculations were performed by using a self-consistent charge procedure,[23] SCC–Xα–DV, where the Coulomb potential is generated by using values derived from a Mulliken population analysis. Density of states plots were calculated as described previously.[11]

Bond distances and angles for theoretical calculations were taken from published crystal structures of $Rh_4(CO)_{12}$ and $Ir_4(CO)_{12}$[3,4] and idealized to C_{3v} and T_d symmetry, respectively. In the rhodium calculations, C–O distances were taken as the average over all 12 such bonds in the cluster. This was required because of the variability in bond lengths from crystal twinning.[3] The $Ir_4(CO)_{12}$ crystal structure was complicated by disorder; in their solution of the structure, Churchill and Hutchinson used fixed C–O distances (1.14 Å) and Ir–C–O angles (180°).[4]

Results and Discussion

Molecular orbital energy level diagrams derived from SCF–Xα–DV calculations of $M_4(CO)_{12}$ (M = Co, Rh, Ir) are presented

(16) Hoffmann, R.; Wijeyesekera, S. D.; Sung, S.-S. *Pure Appl. Chem.* **1986**, *58*, 481–494. Mingos, D. M. P. *Chem. Rev.* **1986**, *15*, 31–61.
(17) Perrin, D. D.; Armarego, W. L. F.; Perrin, D. R. *Purification of Laboratory Chemicals*; Pergamon: Oxford, 1983.
(18) Martinengo, S.; Giordano, G.; Chini, P. *Inorg. Synth.* **1980**, *20*, 209–212.
(19) Demortier, A.; Bard, A. J. *J. Am. Chem. Soc.* **1973**, *95*, 3495–3500.
(20) Smith, W. H.; Bard, A. J. *J. Am. Chem. Soc.* **1975**, *97*, 5203–5210.
(21) Averill, F. W.; Ellis, D. E. *J. Chem. Phys.* **1973**, *59*, 6412–6418.
(22) Mulliken, R. S. *J. Chem. Phys.* **1955**, *23*, 1833–1841.
(23) Rosen, A.; Ellis, D. E.; Adachi, H.; Averill, F. W. *J. Chem. Phys.* **1976**, *65*, 3629–3634.

Table II. Percent Atomic Contributions to Frontier Orbitals of $M_4(CO)_{12}$ Complexes

Co					Rh					Ir			
orbital	ΔE,[a] eV	Co[ap]	Co[ba]	CO[b]	orbital	ΔE,[a] eV	Rh[ap]	Rh[ba]	CO[b]	orbital	ΔE,[a] eV	Ir	CO
28e	0.78	3	19	76,2-μ	28e	0.70	16	1	82	$16t_2$	0.25	17	83
$7a_2$	0.53	0	31	38,30-μ	$7a_2$	0.44	0	15	40,44-μ	9e	0.15	13	87
27e	0	21	45	31,2-μ	27e	0	20	33	45,2-μ	$9t_1$	0	56	44
26e	-1.30	41	37	20,2-μ	$20a_1$	-1.91	6	52	34,8-μ	8e	-2.08	55	45
$20a_1$	-1.89	40	30	26,4-μ	26e	-2.05	20	31	27,22-μ	$8a_1$	-2.32	55	45
$19a_1$	-2.02	3	68	24,5-μ	25e	-2.50	15	36	25,24-μ	$15t_2$	-3.48	61	39
25e	-2.15	40	38	7,15-μ	$19a_1$	-2.73	2	59	30,8-μ	$8t_1$	-5.41	72	28
$6a_2$	-2.32	0	94	5,1-μ	$6a_2$	-3.05	0	85	12,3-μ	$14t_2$	-5.66	71	29
24e	-2.45	27	54	5,14-μ	24e	-3.65	1	72	22,4-μ	$13t_2$	-6.58	73	27
$18a_1$	-2.55	46	42	11	$5a_2$	-3.75	0	91	9	7e	-6.87	71	29
$5a_2$	-2.85	0	76	19,5-μ	23e	-3.80	43	35	15,7-μ	$7a_1$	-7.63	72	28
23e	-2.95	13	58	29,1-μ	$18a_1$	-3.84	50	30	19,1-μ	$7t_1$	-8.38	1	99
22e	-3.15	13	74	7,5-μ	22e	-4.02	1	71	10,19-μ				
$17a_1$	-3.35	9	79	11	21e	-4.52	36	34	11,19-μ				
21e	-3.55	3	80	13,4-μ	$17a_1$	-5.22	29	57	13,1-μ				

[a] ΔE = energy relative to the lowest unoccupied molecular orbital. [b] The terminal carbonyl contribution unless specified μ for the bridging carbonyl groups.

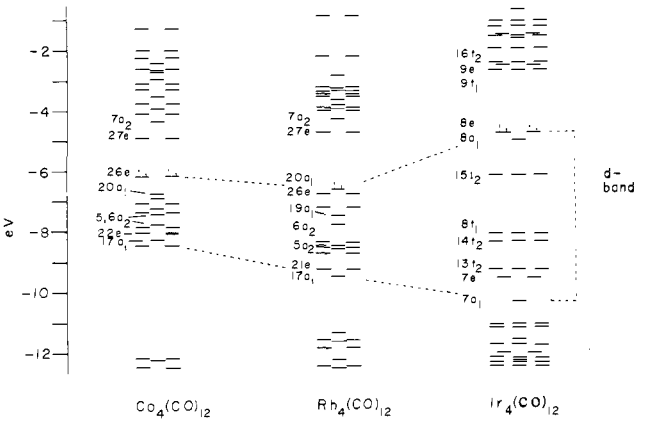

Figure 2. Molecular orbital energy level diagrams for $Co_4(CO)_{12}$, $Rh_4(CO)_{12}$, and $Ir_4(CO)_{12}$ from SCF–Xα–DV calculations.

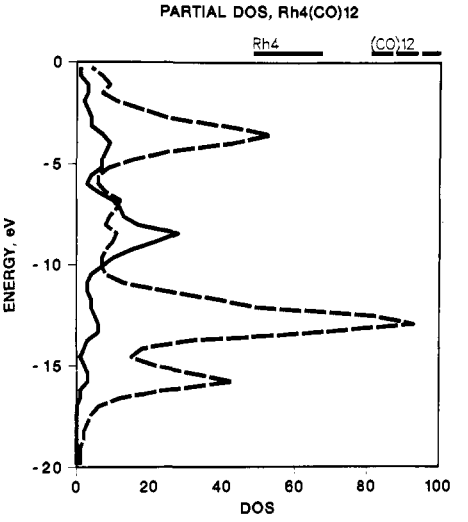

Figure 3. Plot of the partial density of states in $Rh_4(CO)_{12}$: —, Rh_4; ···, $(CO)_{12}$.

in Figure 2. An analysis of the charge distribution in these clusters is listed in Table I along with an atomic breakdown of frontier orbitals in Table II. On the basis of both theoretical and experimental considerations, the highest energy occupied orbitals in $Co_4(CO)_{12}$, from -6 to -3.5 eV, were assigned to Co_4-dominated levels.[11] Occupied orbitals more tightly bound than the metal-based ones are primarly of CO character, as are the cluster of unoccupied orbitals just above the Fermi energy. Density of states (DOS) analyses show small but significant amounts of Co character mixed into both the occupied and unoccupied CO-based levels, while the metal-based levels just below E_f contain a substantial contribution from the CO's, with the net result being delocalized bonding.

A similar qualitative description can be applied to the Rh and Ir clusters. High-lying occupied levels are of dominant metal character, with CO-based levels to higher and lower energy. The DOS plot for $Rh_4(CO)_{12}$ (Figure 3) illustrates some subtle differences from the electronic structure of $Co_4(CO)_{12}$. First, the width of the metal-based band just below E_f has increased from 2.5–3 eV in $Co_4(CO)_{12}$ to 3–3.5 eV in $Rh_4(CO)_{12}$. In addition, the metal-based band is no longer symmetric, having developed a shoulder on the higher energy side at 7 eV. This splitting of the Rh_4 level structure is also evident in the orbital population analysis (Table II). Examination of the MO energy level diagram (Figure 2) suggests that the shoulder in the DOS arises from the splitting between orbitals $20a_1$–$6a_2$ and $24e$–$17a_1$, where we see a ~0.7-eV gap. The $Ir_4(CO)_{12}$ cluster also displays a splitting in its d band, between $8e$–$15t_2$ and $8t_1$–$7a_1$, where now a 2-eV gap has developed. The total d bandwidth for $Ir_4(CO)_{12}$ is larger than that in either Co or Rh, spanning 6 eV.

Broadening of the metal-based band of levels, on progressing Co → Rh → Ir, suggests stronger interactions between the different metal centers. A similar trend has been observed[25] in the UPS spectra of trinuclear Fe, Ru, and Os clusters. Indeed, thermodynamic bond energy data[26] and force constant calculations from vibrational data[27] show a strengthening of the M–M bond as one descends a column in the periodic table. Optical studies of metal–metal bonded dimeric and trimeric systems also show an increase in M–M interactions on descending a homologous series.[28] The calculations exhibit a marked increase in d-band splitting, and presumably increased metal–metal bonding, on progressing from Rh to Ir. This agrees with the great stability of $Ir_4(CO)_{12}$ as compared to $Co_4(CO)_{12}$ or $Rh_4(CO)_{12}$ but must be qualified by including the structural change that occurs (Figure 1). Broadening of the low-energy valence ionizations also results from orbitals with metal–metal antibonding character, which become partly occupied for carbonyl clusters of the late transition metals.[13,25]

Comparison of the calculated DOS and the ultraviolet photoelectron spectrum (UPS)[29] of $Ir_4(CO)_{12}$ shows a great similarity. The experimental spectrum consists of a ~5 eV wide Ir d-based

(24) Holland, G. F.; Ellis, D. E.; Trogler, W. C. *J. Chem. Phys.* **1985**, *83*, 3507–3513.
(25) Chesky, P. T.; Hall, M. B. *Inorg. Chem.* **1983**, *22*, 2998–3007.
(26) Connor, J. A. *Top. Curr. Chem.* **1977**, *71*, 71–106.
(27) Oxton, I. A. *Inorg. Chem.* **1980**, *19*, 2825–2829.
(28) Levenson, R. A.; Gray, H. B. *J. Am. Chem. Soc.* **1975**, *97*, 6042–6047. Levenson, R. A.; Gray, H. B.; Ceasar, G. P. *Ibid.* **1970**, *92*, 3653–3654. Tyler, D. R.; Levenson, R. A.; Gray, H. B. *Ibid.* **1978**, *100*, 7888–7893. Miskowski, V. M.; Smith, T. P.; Loehr, T. M.; Gray, H. B. *Ibid.* **1985**, *107*, 7925–7934. Kostikova, G. P.; Korol'kov, D. V. *Russ. Chem. Rev. (Engl. Transl.)* **1985**, *54*, 344–360.
(29) Plummer, E. W.; Salaneck, W. R.; Miller, J. S. *Phys. Rev. B: Solid State* **1978**, *18*, 1673–1701.

Table III. Volume Integrated Charge of Fragments for $M_4(CO)_{12}$ Clusters

fragment	M		
	Co[a]	Rh	Ir
M_4	+3.11	+5.39	+5.40
Terminal carbonyl, per CO			
apical	−0.18	−0.38	−0.45
basal	−0.27	−0.39	
bridging carbonyl, per CO	−0.34	−0.64	

[a] Reference 11.

band of ionizations, with three resolvable peaks at 7.25, 8.8 and 10.4 eV. If one assumes that all orbitals relax to the same extent on ionization (~2 eV for Co_4 clusters[11]), then the ground-state DOS should mimic an experimental valence photoelectron spectrum. Spin-restricted nonrelativistic ground-state calculations for $Ir_4(CO)_{12}$ with a 0.4-eV broadening factor for the DOS plot exhibit features in the d band similar to those observed experimentally, i.e., a broad (~5–6 eV) group of ionizations with four resolvable peaks at 4.8, 6.0, 8.1 and 9.3 eV. The calculated trend in d-band splitting is confirmed by the UPS spectra, where in $Co_4(CO)_{12}$ a single band is observed[30] with a width of ~2–3 eV. While relativistic effects become important as one progresses from 3d to 5d metals,[31] it appears that the one-electron theory used in these calculations accounts adequately for the disposition of energy levels in $Ir_4(CO)_{12}$. To check these conclusions, we performed a ground-state relativistic calculation for $Ir_4(CO)_{12}$. Since only minor shifts in the orbital scheme were observed, such refinements were not considered further.

In $Co_4(CO)_{12}$, all orbitals in the d band are of 70–80% Co character (Table I), but in $Rh_4(CO)_{12}$ and $Ir_4(CO)_{12}$ there is a higher energy group of levels of 50–60% metal character and a lower energy group of 70–90% metal character. Results for $Ir_4(CO)_{12}$ appear to exaggerate effects seen in the Rh cluster and resemble results obtained from extended Hückel theory (EHT).[32] In that work, Hoffmann and co-workers found the metal-based orbitals split into a weakly interacting, lower energy group of t_{2g}-like levels containing 24 electrons and a higher group of strongly interacting e_g-like levels containing 12 electrons. Results from the Xα–DV calculations also show a division of valence electrons in $Ir_4(CO)_{12}$ into a stable set of 24 and a less stable set of 12. This division correlates with the strength of metal–metal interactions, as judged from the less distinct separation of the d band in $Rh_4(CO)_{12}$ and its continuous appearance in $Co_4(CO)_{12}$. For the three clusters considered here, the $(n + 1)$s,p (n = 3–5) contribution is enhanced in the frontier orbitals. Mixing of s and p character into the predominantly metal d orbitals allows for better metal–metal overlap, as we and others have noted in previous work.[11,13,32] For the clusters $M_4(CO)_{12}$, the highest energy occupied orbitals are of largely metal nd character, with significant admixtures of $(n + 1)$s,p. These orbitals interact strongly and become destabilized with respect to a larger group of levels that contain greater amounts of nd character (but no $(n + 1)$s,p).

Volume-integrated charges proved useful in the analysis of ligand substitution effects on a common Co_4 core.[11] A comparison of atomic and cluster fragment charges (Table III) provides insight into the comparative electronic structure of the units $M_4(CO)_{12}$, where a $(CO)_{12}$ cage is maintained about a metal core that varies from Co to Rh to Ir. The striking feature in comparing these values is the markedly more positive cluster core charge calculated for Rh and Ir. The volume integrated charge amounts to +5.39 and +5.40 for Rh_4 and Ir_4 cores, as compared to +3.11 for Co_4. Carbonyl groups are correspondingly more negative in the Rh and Ir clusters, with the bridging CO's in $Rh_4(CO)_{12}$ undergoing the greatest change in comparison to cobalt. We attribute this to greater M → CO π^* back-bonding. Greater d–π overlap in the second and third transition series makes π-back-bonding more efficient in Rh and Ir. As found previously[11] for substituted Co_4 clusters, charge localization in the carbonyl groups occurs at carbon and not oxygen as expected from the polarization of the CO π^* orbitals toward carbon. In the tetracobalt clusters, substitution of CO with poor π-accepting ligands results in greater negative charge on the metal core and, through M → CO π^*-back-bonding, to the remaining carbonyls.[11]

Although one expects stronger M–CO bonding for Rh and Ir than Co, the magnitude of the difference implied by the volume integrated charges is noteworthy. Reactions between metal carbonyls and Lewis acids occur preferentially at bridging carbonyl groups,[33] which suggests they are more basic than terminal CO groups. As far as we are aware, there has not been a systematic investigation of Lewis acid affinities as a function of metal for a family of related cluster carbonyls. We predict that examination

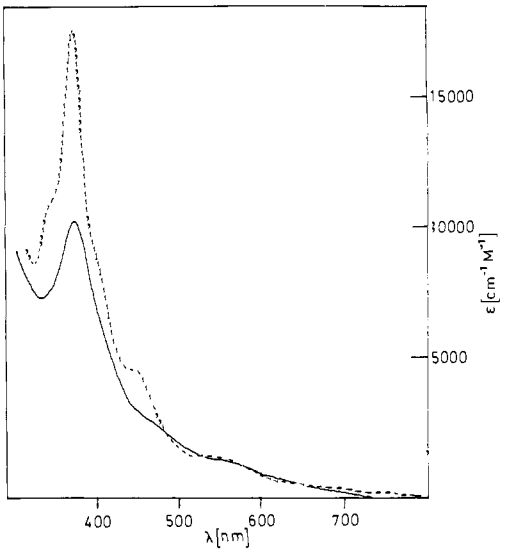

Figure 4. Electronic absorption spectra of $Co_4(CO)_{12}$ in 2-methylpentane solvent. The solid line shows the spectrum at room temperature and the dashed line at 77 K. The ϵ for the 77 K spectrum was not corrected for solvent contraction.

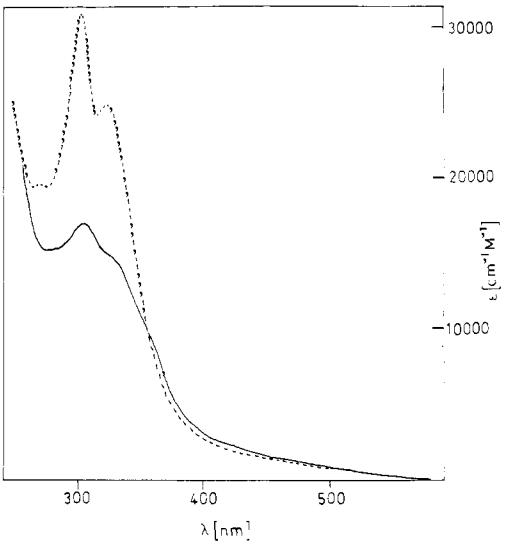

Figure 5. Electronic absorption spectra of $Rh_4(CO)_{12}$ in 2-methylpentane solvent. The solid line shows the spectrum at room temperature and the dashed line at 77 K. The ϵ for the 77 K spectrum was not corrected for solvent contraction.

(30) Green, J. C.; Mingos, D. M. P.; Seddon, E. A. *Inorg. Chem.* **1981**, *20*, 2595–2602.
(31) Rosen, A.; Ellis, D. E. *J. Chem. Phys.* **1975**, *62*, 3039–3048. Ellis, D. E. In *Actinides in Perspective*; Edelstein, N. M., Ed.; Pergamon: Ltd: New York, 1982; pp 123–143. Pitzer, K. S. *Acc. Chem. Res.* **1979**, *12*, 271–276. Pyykkö, P.; Desclaux, J.-P. *Acc. Chem. Res.* **1979**, *12*, 276–281.
(32) Hoffmann, R.; Schilling, B. E. R.; Bau, R.; Kaesz, H. D.; Mingos, D. M. P. *J. Am. Chem. Soc.* **1978**, *100*, 6088–6093. Miessner, V. H. *Z. Anorg. Allg. Chem.* **1983**, *505*, 187–194.
(33) Kristoff, J. S.; Shriver, D. F. *Inorg. Chem.* **1974**, *13*, 499–506.

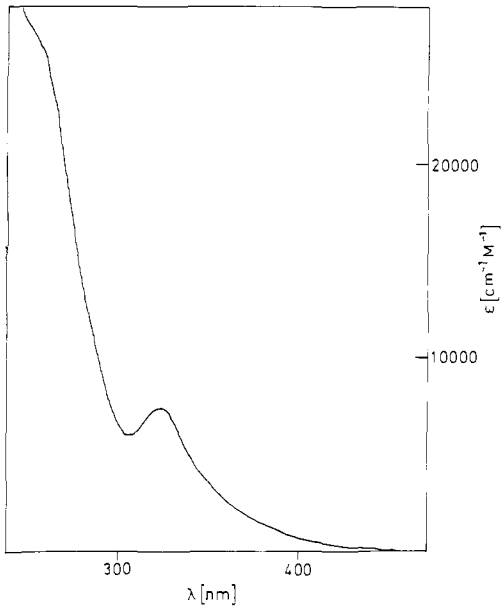

Figure 6. Electronic absorption spectrum of $Ir_4(CO)_{12}$ in CH_2Cl_2 at room temperature.

of the Co–Rh–Ir system under consideration here should show the bridging carbonyls of $Rh_4(CO)_{12}$ to be substantially more basic than bridging carbonyl groups in $Co_4(CO)_{12}$ or terminal carbonyl groups in $Ir_4(CO)_{12}$.

Electronic Absorption Spectra. The electronic absorption spectra of $Ir_4(CO)_{12}$, $Rh_4(CO)_{12}$, and $Co_4(CO)_{12}$ are shown in Figures 4–6, respectively. To understand these spectra, we first analyze the highest symmetry molecule, $Ir_4(CO)_{12}$, and then treat the C_{3v} clusters $Rh_4(CO)_{12}$ and $Co_4(CO)_{12}$ as perturbed analogues. Given the similarities among these spectra (Figures 4–6) and those of tripod-substituted clusters (Table IV), we conclude that the effects of (1) varying the metal, (2) the presence of bridging carbonyl groups, and (3) coordination of the capping tripod ligand do not greatly perturb the optical spectra of $M_4(CO)_{12}$-based clusters. Differences observed in these spectra may be attributed to variations in the strength of M–M and M–CO interactions.

The electronic absorption spectra in Figures 4–6 may be divided into regions of high-energy UV ($\lambda < 300$ nm), low-energy UV (300 nm $< \lambda <$ 370 nm), and visible energies ($\lambda > 370$ nm). Each cluster displays an intense ($\epsilon > 30\,000$ M^{-1} cm^{-1}) absorption around 245 nm, a low-energy UV absorption at ~300–375 nm with $\epsilon \approx 10\,000$ M^{-1} cm^{-1}) and a long absorption tail into visible wavelengths. For the dodecacarbonyl clusters the low-energy UV maximum sharpens and blue shifts slightly on cooling, similar to the $\sigma \rightarrow \sigma^*$ transitions in $M_2(CO)_{10}$ and $M_3(CO)_{12}$ systems.[28] We propose the absorption in these tetranuclear clusters also involves a transition between metal–metal bonding and antibonding orbitals.

Previous spectroscopic studies of mono-,[34] di-,[28] and trinuclear[13,28] metal carbonyls show that an intense metal → CO (MLCT) transition occurs between 260 and 230 nm regardless of cluster size or the metal involved. On this basis, the absorptions at 250 nm in $Ir_4(CO)_{12}$ and 232 nm in $Co_4(CO)_{12}$ are assigned to MLCT transitions. This is supported by the assignment of the spectrum of $Co_2(CO)_8$, which places an MLCT absorption at 243 nm,[35] as well as by the assignment of the spectrum of $Co(CO)_4^-$, which places an MLCT absorption at 250 nm.[35] Transitions below 285 nm are obscured by an intense absorption for $Rh_4(CO)_{12}$.

Optical transitions in these clusters can be understood in the context of the molecular orbitals near the Fermi energy (Table II and Figure 2). The highest occupied group of orbitals consists predominantly (50–70%) of metal character for all clusters studied here. The high metal content (50–60%) of the LUMO in comparison to the other unoccupied orbitals suggests it is the unoccupied orbital involved in the metal–metal localized transitions observed between 375 and 300 nm.

For $Ir_4(CO)_{12}$, the allowed transition $8e \rightarrow 9t_1$ (2 eV, 620 nm) and the forbidden transition $8a_1 \rightarrow 9t_1$ (2.3 eV, 540 nm) are calculated to lie lowest in energy. No well-resolved absorptions are observed at the calculated energies. We suggest that these two low-energy transitions, together with other low-lying transitions, e.g., $8e$, $8a_1 \rightarrow 9e$, $16t_2$, contribute to the long visible tail from the peak at 321 nm. From the metal content of the LUMO and energetic considerations, the metal–metal localized transition at 321 nm is assigned as $15t_2 \rightarrow 9t_1$. The energy calculated for this transition, 3.5 eV (350 nm), lies within 10% of the experimental value (3.89 eV). Because EHT calculations[32] found t_1 orbital combinations to be antibonding with e and t_2 bonding, the transition $15t_2 \rightarrow 9t_1$ should exhibit $\sigma \rightarrow \sigma^*$ character.

Analogous spectral assignments are proposed for $Co_4(CO)_{12}$ and $Rh_4(CO)_{12}$, whose $7a_2 + 27e$ LUMO's correlate with $9t_1$ in $Ir_4(CO)_{12}$. Visible absorptions are attributed to transitions from the top of the occupied metal-based band into the LUMO and nearby more CO-localized orbitals. Assignment of the metal–metal based transition in each case is less straightforward than for $Ir_4(CO)_{12}$. If we assume this transition populates the cluster LUMO (in each case of e symmetry), and recalling that $I \approx \langle \phi_{init} | e\hat{r} | \phi_{final} \rangle$, we find that in C_{3v} symmetry, $a_1 \rightarrow e$ and $a_2 \rightarrow e$ transitions are allowed only with (x,y) polarization, while $e \rightarrow e$ transitions are allowed in all polarizations. With an eye toward maximizing excited- and ground-state orbital overlap, we find that (restricting our discussion to metal, M, d orbitals only):

$$a_1 = M^{ap}(d_{z^2}) + M^{ba}[(d_{xz,yz}) + (d_{xy,x^2-y^2}) + d_{z^2}]$$

$$a_2 = M^{ba}[(d_{xz,yz}) + (d_{xy,x^2-y^2})] \text{(no apical contribution)}$$

$$e = M^{ap}[(d_{xz,yz}) + (d_{xy,x^2-y^2})] + M^{ba}[(d_{xz,yz}) + (d_{xy,x^2-y^2}) + d_{z^2}]$$

Given that an e orbital is populated in this intense transition, maximum orbital overlap, and hence maximum transition intensity, would arise from an allowed $e \rightarrow e$ excitation from an occupied orbital of similar atomic composition to the LUMO.

In $Co_4(CO)_{12}$ the atomic composition of the orbital 22e closely resembles that of the LUMO, 27e. Both orbitals contain large amounts of d_{xz}, d_{yz} character at both apical and basal cobalts, leading to bonding localized along the tetrahedral faces. The importance of bonding in the tetrahedral faces, as opposed to edges and vertices, has been discussed by Hoffmann and co-workers.[32] An optical transition, $22e \rightarrow 27e$ calculated at 3.15 eV (393 nm), compares favorably with one observed at 3.3 eV (375 nm). Consistent with the degenerate component proposed for this transition, a strong A term was observed in the MCD spectrum of $Co_4(CO)_{12}$ at 370 nm. Other occupied orbitals at energies near 22e do not resemble the LUMO in orbital composition and seem unlikely candidates for the metal–metal excitation.

We tentatively propose a $21e \rightarrow 27e$ assignment for the metal-localized absorption in $Rh_4(CO)_{12}$. The observed energy of 4.09 eV (303 nm) compares well with the calculated value of 4.52 eV. The next best assignment would be the $26e \rightarrow 27e$ excitation, calculated at 2.05 eV. From energetic considerations, this choice appears less likely than $21e \rightarrow 27e$, in spite of the good overlap expected between ground- and excited-state wave functions. As a final comment, if one examines orbitals such as $20a_1$, $19a_1$, 24e, and 22e, where the metal contribution is localized in the basal plane, it appears that a model of a triangular Rh_3 fragment perturbed by the apical Rh might be more appropriate.

Other trends observed for metal carbonyl dimers and trimers are also seen in the tetranuclear series. As one descends a family in the periodic table, the overlap between two metal atoms should increase because the orbitals become larger. In the di- and trinuclear carbonyls the energy of the $\sigma \rightarrow \sigma^*$ transition increases in the same order.[28] This was attributed to the increasing overlap that causes a greater separation of the bonding and antibonding orbitals. The ordering for the tetranuclear clusters is Co < Ir < Rh, a reversed order of Ir and Rh from that expected. We

(34) Beach, N. A.; Gray, H. B. *J. Am. Chem. Soc.* **1963**, *85*, 2922–2927.
(35) Frazier, C. C., III Ph.D. Thesis, California Institute of Technology, 1976.

Table IV. Electronic Absorption Spectral Data for Band Maxima in $M_4(CO)_{12}$ and $M_4(CO)_9$(tripod) Clusters

cluster	λ, nm (ε)	cm^{-1}	eV
$Co_4(CO)_{12}$	660 (1300)	15 200	1.85
	540 (3000)	19 200	2.29
	460 (5500)	22 000	2.69
	375 (19 000) $\sigma \rightarrow \sigma^*$	26 700	3.31
	340 (13 000)	29 000	3.65
$Rh_4(CO)_{12}$	303 (16 600) $\sigma \rightarrow \sigma^*$	33 000	4.09
$Ir_4(CO)_{12}$	321 (7500) $\sigma \rightarrow \sigma^*$	31 200	3.87
	250 (31 300)	40 000	4.96
$Co_4(CO)_9$(tripod)	760 (1100)	13 200	1.61
	595 (4600)	16 800	2.06
	450 sh (4200)	22 200	2.72
	380 (11 800) $\sigma \rightarrow \sigma^*$	26 300	3.22
	265 (40 000)	37 700	4.62
$Rh_4(CO)_9$(tripod)	500 sh (3700)	20 000	2.48
	380 (13 000) $\sigma \rightarrow \sigma^*$	26 300	3.26
	290 sh	34 500	4.27
$Ir_4(CO)_9$(tripod)	342 (4400) $\sigma \rightarrow \sigma^*$	29 200	3.62
	292 (13 000)	34 200	4.24

attribute this to structural differences between $Rh_4(CO)_{12}$ and $Ir_4(CO)_{12}$. First, lowering the symmetry from T_d in $Ir_4(CO)_{12}$ to C_{3v} in $Rh_4(CO)_{12}$ should split the metal–metal transition $15t_2 \rightarrow 9t_1$ into $a_1 + e \rightarrow a_2 + e$ combinations. Second, a previous study[35] of $Co_2(CO)_8$ showed that the $\sigma \rightarrow \sigma^*$ transition of the bridged isomer occurred at much higher energy than the corresponding transition in the unbridged isomer, and $Ir_4(CO)_{12}$ contains no bridging carbonyl groups, unlike $Co_4(CO)_{12}$ and $Rh_4(CO)_{12}$. Thus, compared to the latter molecules, the "$\sigma \rightarrow \sigma^*$" transition in $Ir_4(CO)_{12}$ should be displaced to lower energy, which accounts for the anomalous ordering.

Phosphine substitution effects on the energy of the $\sigma \rightarrow \sigma^*$ transition are unpredictable in the di- and trinuclear carbonyl compounds.[28] With monodentate phosphines we find a similar behavior for the tetranuclear carbonyls. Triphenylphosphine substitution in $Rh_4(CO)_{12}$ to give $Rh_4(CO)_{10}(PPh_3)_2$ lowers the energy of the "$\sigma \rightarrow \sigma^*$" transition from 303 to 370 nm. However, the $\sigma \rightarrow \sigma^*$ transition shifts from 320 nm in $Ir_4(CO)_{12}$ to 310 nm in $Ir_4(CO)_9(PPh_3)_3$. Again, an MCD A term is observed for the transition assigned to $\sigma \rightarrow \sigma^*$. These opposite shifts emphasize that several factors may control the energy of the $\sigma \rightarrow \sigma^*$ excitation. In contrast to the monodentate phosphines, coordination of the tripod phosphine $(PPh_2)_3CH$ to all the $M_4(CO)_{12}$ clusters decreases the energy of the "$\sigma \rightarrow \sigma^*$" excitation (Table IV).

For M = Co, the red-shift of this "$\sigma \rightarrow \sigma^*$" transition on tripod substitution is only 350 cm^{-1}, but for M = Rh and Ir, the shift is greater at ~6000 and 1800 cm^{-1}, respectively. Coordination of the donor ligand tripod increases the electron density of the M_4 core. The stronger M–M interactions in the Rh_4 and Ir_4 clusters are more perturbed by this electron donation than the weakly interacting Co_4 centers. Tripod substitution destabilizes occupied bonding levels and stabilizes the corresponding unoccupied, "antibonding", levels and red shifts the transitions between these orbitals. The difference observed for coordination of tripod and monodentate phosphines may be attributed to the presence of bridging carbonyls in the $Ir_4(CO)_{12-n}L_n$ clusters. The cluster $Ir_4(CO)_9$(tripod) does not contain bridging carbonyls.[10]

Electrochemistry. Cyclic voltammetric (CV) studies of the family of $M_4(CO)_9$(tripod) clusters show different electrochemical behavior when M = Co is compared to M = Rh and Ir. While the cobalt cluster undergoes reversible one-electron reduction (−0.78 vs. AgRE) and oxidation (+0.94 vs. AgRE), coupled chemical reactions complicate the electron transfer process for the rhodium and iridium analogues (as also observed in $Rh_4(CO)_{12}$). Redox data are summarized in Table V.

Good correlation was obtained between electrochemical reduction potentials and cluster core charges derived from calculations for a series of tetracobalt clusters.[11] We note that the

Table V. Cyclic Voltammetric Data for $M_4(CO)_{12}$ and $M_4(CO)_9$(tripod) on Cathodic Scans

cluster	$E_{pc}(1)$, V	n	$E_{pc}(2)$, V	n
$Co_4(CO)_9$(tripod)[b]	−0.780[e]	1	−1.49	1
$Rh_4(CO)_9$(tripod)[b]	−1.138	1	≤−1	1
$Ir_4(CO)_9$(tripod)[b]	−1.82	~1		
$Ir_4(CO)_9$(tripod)[c]	−1.70	~1	−2.10	~1
$Co_4(CO)_{12}$[c]	−0.12			
$Rh_4(CO)_{12}$[d]	−0.80		−1.26	

[a] Scan rate = 200 mV/s with IR compensation; potentials reported vs. AgRE; n values from coulometry experiments. [b] 0.2 M $TBABF_4/CH_2Cl_2$ solution, data for cobalt from ref 11. [c] 0.2 M $TBABF_4$/THF solution. [d] 0.2 M $TBABF_4$/THF solution with 1 atm of CO. [e] Value given is $E^{\circ\prime}$.

cluster core charge–reduction potential correlation does not hold in comparing the tetrametallic clusters examined here (Tables III and V); the rhodium and iridium clusters undergo reduction at more negative potentials than would be predicted by the trend in cluster core charges. We suggest that the changing metal–metal interactions spoil the correlation. Cluster core charges, while effective in describing changing metal–ligand interactions at a common metal core, are by their nature insensitive to changes in covalent metal–metal bonding.

Conclusions. Some generalizations can be made about the electronic structures of Co_4, Rh_4, and Ir_4 clusters. (1) The magnitude of metal–metal interactions increases as one descends the group, Co to Rh to Ir. This is predicted based on DOS analyses derived from SCF–Xα–DV calculations and is confirmed directly in valence photoelectron spectroscopic studies. These stronger interactions are also manifested in a blue shift of the "$\sigma \rightarrow \sigma^*$" electronic absorption band, as the more bonding metal orbitals are stabilized and more antibonding orbitals destabilized. (2) Volume integrated charges from SCF–Xα–DV calculations suggest that the strength of metal–CO back-bonding should also increase as the group is descended since the Rh_4 and Ir_4 cores are considerably more positive than the Co_4 cores. (3) The value of the first reduction potential, $E^{\circ}(1)$, becomes more negative as one descends the group from Co to Ir. This is in qualitative agreement with results of Fenske[36] and Bursten,[37] where redox potentials for mononuclear complexes were seen to correlate well with frontier orbital energies. In contrast to previous work on related Co_4 clusters, good correlation was not observed between the first reduction and cluster core charges obtained from a volume integrated charge analysis. Using electrochemical redox potentials as an estimate for cluster core charge does not seem effective when comparing different metal cores. The effect of changing M–M and M–CO bonding on redox potentials requires a description beyond the simple core charge–redox potential correlation.

Acknowledgment. This material is based on work supported by the National Science Foundation under Grants No. CHE-85-04088 to W.C.T., CHE-84-19828 to H.B.G. and DMR-82-14966 to D.E.E. W.C.T. thanks the Alfred P. Sloan Foundation for a research fellowship. We thank P. J. Stephens of the University of Southern California for allowing us access to his MCD equipment. We thank J. A. Ibers for the use of electrochemical equipment. G.F.H. thanks J. G. Gaudiello and M. C. Manning and D. F. Shriver and his research group for helpful suggestions. This is Contribution No. 7556 from the Arthur Amos Noyes Laboratory.

Registry No. $Co_4(CO)_{12}$, 17786-31-1; $Rh_4(CO)_{12}$, 19584-30-6; $Ir_4(CO)_{12}$, 18827-81-1; $Co_4(CO)_9$(tripod), 75801-99-9; $Rh_4(CO)_9$(tripod), 75790-10-2; $Ir_4(CO)_9$(tripod), 75790-09-9.

(36) Sarapu, A. C.; Fenske, R. F. *Inorg. Chem.* **1975**, *14*, 247–253.
(37) Bursten, B. E. *J. Am. Chem. Soc.* **1982**, *104*, 1299–1304. Bursten, B. E.; Darensbourg, D. J., Kellogg, G. E.; Lichtenberger, D. L. *Inorg. Chem.* **1984**, *23*, 4361–4365.